Hindawi
Journal of Chemistry
Volume 2021, Article ID 5519411, 14 pages
https://doi.org/10.1155/2021/5519411

Research Article

A Study of 1-Benzyl-3-phenyl-2-thiourea as an Effective Steel Corrosion Inhibitor in 1.0 M HCl Solution

Quy Huong Dinh,[1] **Tran Duong**,[1] **and Nam Pham Cam**[2]

[1]*Department of Chemistry, University of Education, Hue University, Hue 530000, Vietnam*
[2]*Department of Chemical Engineering, The University of Danang–University of Science and Technology, Danang 550000, Vietnam*

Correspondence should be addressed to Quy Huong Dinh; dqhuong@hueuni.edu.vn

Received 22 February 2021; Revised 16 April 2021; Accepted 29 April 2021; Published 8 May 2021

Academic Editor: Liviu Mitu

1-Benzyl-3-phenyl-2-thiourea (BPTU) was studied as a steel corrosion inhibitor in 1.0 M HCl solution. Experimental methods were conducted including potentiodynamic polarization measurement (PPM), electrochemical impedance spectroscopy (EIS), and scanning electron microscopy (SEM) analysis. Quantum calculations were performed at B3LYP/6-311G(d,p). Hexamethylenetetramine (URO) was selected for comparison with BPTU. The results showed that BPTU with the concentration of 2×10^{-4} M and at the temperature of 30°C could protect the steel surface with the highest inhibition efficiency of 94.99% and 94.30% according to EIS and PPM, respectively. High temperature decreased BPTU's ability to inhibit the steel corrosion. The adsorption of BPTU on the steel surface is followed by the modified Langmuir isotherm. Quantum chemical calculations showed that the thiourea functional group is the main adsorption center of BPTU. The experimental results are completely consistent with theoretical calculations.

1. Introduction

The molecular structure of a compound determines the chemical properties of that compound. Substances containing heteroatoms such as N, O, S and benzene rings in the molecule are often used as metal corrosion inhibitors [1–4]. These heteroatoms possess high electron density, and they tend to donate easily electrons to the metal surface. Therefore, these compounds can adsorb on the metal surface. Besides, the presence of benzene rings in the molecule increases the electrostatic interaction between inhibitors and metal surfaces [5], helping to enhance metal corrosion inhibition for a long time; thus, it is an important factor to consider.

Metal corrosion has many serious consequences for the economy. Therefore, the search for cheap and effective metal corrosion inhibitors has attracted the attention of scientists. Thiourea derivatives are particular examples of corrosion inhibitors. In 2012, Li et al. researched the steel inhibition effect of allyl thiourea in 1.0 M H_3PO_4 solution. Its performance was higher than 95% at 20 ÷ 50°C [6]. In 2014, Torres et al. investigated the corrosion inhibition ability of 1,3-dibenzylurea, 1,3-dibenzylthiourea, and 1-benzyl-3-diisopropylthiourea [7]. The results showed that the sulfur atom might play an important role in the inhibition process of the thiourea derivatives for carbon steel corrosion in an acid medium. In 2017, Guo et al. [8] found out the inhibition mechanism of three thiourea derivatives, (1-(4-methoxyphenyl)-3-(4-phenylthiazol-2-yl)thiourea, 1-benzyl-3-(4-phenylthiazol-2-yl)thiourea, and 1-(2-hydroxyethyl)-3-(4-phenylthiazol-2-yl)thiourea), by density functional theory and molecular dynamics simulation. The factors such as solvent, temperature, and coverage were investigated. These results were accordant with the experimental results of Fouda and Soliman [9]. In 2018, two newly -synthesized thioureas were 1-N-(10-(10,20,40-triazole))acetyl-4-N-benzoylthiosemicarbazide and 1-N-(10-(10,20,40-triazole)) methyl-4-N-(300,500- dimethyl)benzoylthiosemicarbazide

[10]. The steric hindrance of the methyl group was suggested as the main influencing factor on the inhibition efficiency of these thioureas. In 2019, N-phenylthiourea was chosen as a mild steel corrosion inhibitor in acid and salt solution [11]. The experimental and theoretical study showed that the adsorption was the main mechanism of N-phenylthiourea to protect the steel surface from the corrosive agents in solution.

Undoubtedly, up to now, thiourea derivatives have been considered as a class of potential inhibitors by many scientists all over the world. The discovery of effective thiourea derivatives is always a driving force for the research of scientists. 1-Benzyl-3-phenyl-2-thiourea (BPTU) is a thiourea derivative which contains benzene rings and polar groups. Its inhibition efficiency is related to the polar functions, acting as active centers for the adsorption. In addition, the presence of multiple benzene rings may increase the molecular coverage density. Therefore, BPTU is expected to become a potential corrosion inhibitor. Besides, hexamethylenetetramine (URO), which is considered as a reference corrosion inhibitor [12–15] was also investigated in the same conditions in order to compare and evaluate the corrosion inhibition ability of BPTU. Experimental methods were used including electrochemical impedance spectroscopy (EIS), potentiodynamic polarization measurement (PPM), and scanning electrochemical microscopy (SEM). Quantum chemical calculations and molecular dynamics simulation were manipulated to provide a theoretical explanation for the corrosion inhibition ability of the studied compounds.

2. Experimental

2.1. Electrodes. Low carbon steel electrode gave a percentage weight content of 0.28% C, 0.40% Si, 1.11% Mn, 0.03% P, 0.012% S, 0.02% S, and 98.148% Fe. Its surface area was 0.196 cm^2; the rest was covered with layers of epoxy to isolate the environment. The electrode surface was smoothed with metallographic emery increasing fineness from 120 to 2000 grits.

2.2. Chemicals. BPTU, HCl, and URO were purchased from Adamas Reagent Co., Ltd. The prepared BPTU concentrations were 10^{-5}, 5×10^{-5}, 10^{-4}, 2×10^{-4} M. Ethanol was added into the solution to ensure the solubility of inhibitors. The 1.0 M HCl blank solution was prepared by diluting the analytical grade 37% with distilled water.

2.3. Electrochemical Impedance Spectroscopy (EIS). EIS tests were measured in a frequency range of 0.01 to 100 kHz. The experiments were conducted after the steel samples were exposed to the medium at room temperature in one hour. The EIS was measured by the Zahner Elektrik electrochemical meter of Germany. Afterwards, Thales 4.5 software was used to simulate the impedance lines and analyze experimental results.

The corrosion inhibition efficiency obtained from the EIS method is calculated according to equation (5) [16–18]:

$$H\% = \frac{R_{ct(inh)} - R_{ct}}{R_{ct(inh)}} \cdot 100, \quad (1)$$

where R_{ct} (Ωcm^2) and $R_{ct(inh)}$ (Ωcm^2) represent charge-transfer resistances without and with the inhibitor.

An equivalent circuit model is provided to describe accurately the impedance lines, in which CPE is a constant element instead of the double-layer capacitance (C_{dl}) in Randles circuit. The impedance of CPE can be calculated using the following equation [19]:

$$Z_{CPE} = Y_o^{-1} \cdot (j\omega)^{-n}, \quad (2)$$

where ω is the angular frequency ($\omega = 2\pi f$, f is the frequency), j is the virtual unit, Y_o is the value of CPE, and n is the compression ratio. n equals 1 when the electrode surface is homogeneous and flat. The value of C_{dl} can be estimated according to the following equation [20]:

$$C_{dl} = Y_o \cdot (\omega_{max})^{n-1}, \quad (3)$$

in which

$$\omega_{max} = 2\pi f_{max}. \quad (4)$$

2.4. Potentiodynamic Polarization Measurement (PPM). PPM was conducted on CPAiocHH5B meter of the Vietnam Academy of Science and Technology with a three-electrode system, in which low carbon steel was a working electrode (WE), Ag/AgCl in saturated KCl (SCE) was a comparison electrode, and stainless steel was a counter electrode (CE). The potential of polarization curves was scanned from −1.00 V to 0.20 V. The temperature of the studied system was adjusted by Memmert Waterbath WNB 45 from 30 to 60°C.

The corrosion inhibition efficiency (H%) is calculated by the following formula [21, 22]:

$$H\% = \frac{i_{corr} - i_{inh}}{i_{corr}} \cdot 100, \quad (5)$$

where i_{corr} is uninhibited corrosion current density ($mA.cm^{-2}$) and i_{inh} is inhibited corrosion current density ($mA.cm^{-2}$).

From corrosion inhibition efficiency, surface coverage is calculated as follows [23]:

$$\theta = \frac{i_{corr} - i_{inh}}{i_{corr}}. \quad (6)$$

The relationship between adsorption free energy (ΔG^0_{ads}) and adsorption constant (K_{ads}) is described by equation (3) [24]:

$$\Delta G^0_{ads} = -RT \ln(55.5\, K_{ads}), \quad (7)$$

in which the value of 55.5 is the molar concentration of water in the solution (M), T is the temperature of the system (K), and R is the gas constant.

Standard adsorption entropy (ΔS^0_{ads}) is calculated using thermodynamic equation (4) [25]:

$$\Delta S^0_{\text{ads}} = \frac{\Delta H^0_{\text{ads}} - \Delta G^0_{\text{ads}}}{T}, \quad (8)$$

where $\Delta \mathbf{H^0_{ads}}$ is the standard enthalpy of the adsorption process.

2.5. Scanning Electrochemical Microscopy (SEM). Steel samples were dipped into 50 mL of 1.0 M HCl without and with inhibitors at their optimum concentration (2×10^{-4} M) for 24 hours. Thereafter, they were washed, dried, and conducted for surface morphological measurements with the JSM-6010PLUS/LV SEM model.

2.6. Quantum Chemical Calculations. Gaussian 09 suit of the program has been applied to carry out quantum chemical calculations through the density functional theory (DFT) method [26]. On the basis of the fundamental laws of quantum mechanics, Gaussian software can be used to calculate the energy, molecular structure, vibrational frequency of molecular systems, and many other molecular properties. In this work, inhibitor molecule structures were optimized at B3LYP functional with a 6-311G(d,p) basis set. Besides, quantum chemical parameters were calculated in this same method [27–31].

2.7. Molecular Dynamics Simulation. Materials Studio 8.0 software was used to carry out molecular dynamic simulation when the inhibitor molecules approach the Fe (110) surface [32]. The $DMol_3$ geometry optimizations of inhibitors were performed by B3LYP functional with DNP basis set and basis file of 3.5. The dimensions of a simulation box were $41.15 \times 36.58 \times 29.97$ Å^3. A simulation time was 500 ps with a time step of 0.1 fs.

In simulated corrosion solution, the molar ratio between H_2O and HCl was 500 : 9 [33]. Thus, the proportion of additional components included 1 inhibitor molecule/491 water molecule/9 hydronium ions/9 chloride ions in the system. However, in the case of the protonated inhibitor molecule, this proportion varied slightly, including 1 protonated inhibitor/492 water/8 hydronium ions/9 chloride ions. The simulation conditions were set up at 303K under canonical ensemble (NVT).

The binding energy (E_{bind}) and interaction energy (E_{int}) between the inhibitor and the Fe (110) surface could be calculated as follows [34]:

$$E_{\text{inter}} = E_{\text{tot}} - \left(E_{\text{surf+sol}} + E_{\text{inh}}\right), \quad (9)$$

$$E_{\text{bind}} = -E_{\text{int}}, \quad (10)$$

in which E_{tot} was the total energy of the entire system, $E_{\text{surf+sol}}$ was the total energy of the Fe (110) surface and the solution without inhibitors, and E_{inh} was the energy of the inhibitor.

3. Results and Discussion

3.1. Effect of Concentration on Inhibition Efficiencies of BPTU

3.1.1. Electrochemical Impedance Spectroscopy (EIS). EIS spectra were applied to study the corrosion inhibition ability of BPTU (Figure 1). As can be seen, all curves show a typical Nyquist diagram with single semicircles shifted along the real impedance of the x-axis. This indicates that double-layer behavior and the charge-transfer of the corrosion process primarily control the corrosion of low carbon steel [28].

As the concentration increases, the radius of the semicircular lines increases. In general, the shape of the semicircular lines in the presence of inhibitor does not change from that of the blank (1.0 M HCl solution). This proves that the mechanism of the corrosion process does not change in the presence of BPTU.

For better visualization of the inflection points of the impedance module as well as the phase angle variation, Bode and phase angle plots are also analyzed and depicted in Figure 2 [18]. The value of the phase angle increases significantly as the inhibitor concentration increases. It is worth noting that the phase angle values of the blank and the inhibitor samples are always lower than −90°, which proves that the capacitor is nonideal [35].

Figure 3 is a representative of example simulation of Nyquist and Bode plots recorded for low carbon steel in 1.0 M HCl without and with 2.10^{-4} M BPTU. In general, the experimental lines and the simulated lines are quite similar. This is demonstrated by the low chi-square values (χ^2) (Table 1) using Thales 4.5 software. It means that this simulation is consistent with experimental data.

An equivalent circuit is shown in Figure 4 to analyze the impedance curves. Based on this circuit, the impedance parameters are calculated. Charge resistance (R_{ct}), solution resistance (R_{s}), and double-layer capacitance (C_{dl}) values are listed in Table 1.

As can be seen, n values change with the different concentrations of BPTU; this indicates that the surface inhomogeneity mutates as a result of the inhibitor's adsorption [36]. Besides, an increase of R_{ct} values and a decrease of C_{dl} values prove that BPTU molecules form a protective layer on the electrode surface to prevent the mass and charge-transfer [23]. According to the EIS method, the inhibition efficiencies of BPTU are 94.99%, 92.43%, 90.90%, and 87.72% at the concentrations of 2×10^{-4} M, 10^{-4} M, 5×10^{-5} M, and 10^{-5} M, respectively.

3.1.2. Open Circuit Potential (OCP). The alteration of OCP over time for low carbon steel in 1.0 M HCl at different concentrations of BPTU at 30°C is shown in Figure 5. In the presence of BPTU, the OCP tends to shift towards negative potentials. The drop of OCP during the first 3000 seconds may be due to the dissolution of the oxide layer that formed previously when the low carbon steel contacted with the

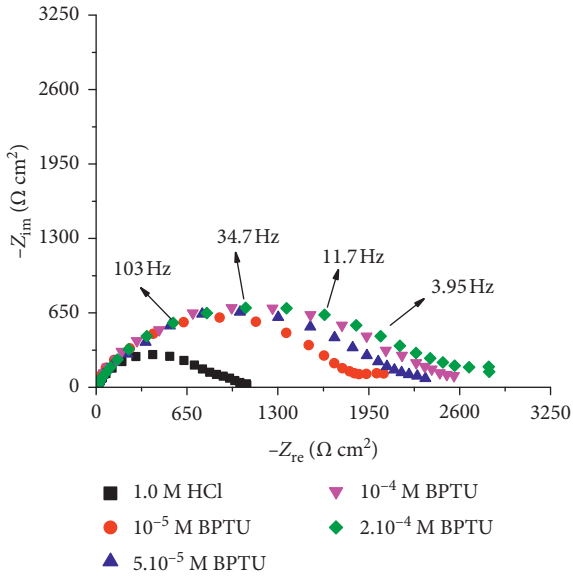

Figure 1: Nyquist plots for low carbon steel in 1.0 M HCl without and with different concentrations of BPTU.

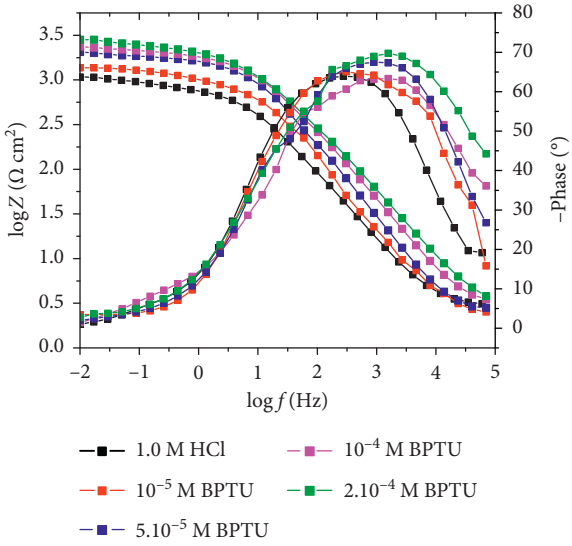

Figure 2: Bode and phase angle diagram for low carbon steel in 1.0 M HCl without and with different concentrations of BPTU.

atmosphere [37]. Therefore, the immersion time of one hour is chosen to reach a certain state for potentiodynamic polarization measurements.

3.1.3. Potentiodynamic Polarization Measurements (PPM). The steel corrosion inhibition ability of BPTU was also investigated by PPM. Figure 6 shows that the cathode branches lie parallel, while the anode branches are nearly overlapping. This proves that BPTU does not change the mechanism of hydrogen reduction and the hydrogen evolution is still controlled by the active site [38]. Some other findings from Table 2 are that the values of β_a change slightly while β_b values change significantly. This indicates that the inhibitor prominently inhibits the cathodic reactions.

Figure 6 shows that the polarization curves of low carbon steel are influenced by the concentration of inhibitor. The higher the inhibitor concentration, the lower the polarization curves. The data in Table 2 show that when the concentration of BPTU varies from 10^{-5} M to 2×10^{-4} M, its corrosion inhibition efficiencies also increase from 88.15% up to 94.30%. These results are quite similar to the efficiencies obtained from the measurements of EIS.

3.2. Comparing Low Carbon Steel Corrosion Inhibition Ability of BPTU with URO. URO has been considered as a traditional inhibitor, so it is selected as an object for comparison and evaluation of steel corrosion inhibition ability of BPTU in 1.0 M HCl solution. Figure 7 shows that the polarization curve of steel in the presence of BPTU is lower than in the presence of URO, which proves that BPTU has better corrosion inhibition than URO. The inhibition performance of URO at 2.10^{-4} M is only 46.57% at 30°C (Table 2). The cage structure of URO impedes its adsorption onto the metal surface [12]. That is the reason that its inhibition efficiency is lower than BPTU.

3.3. Effect of Temperature on Inhibition Efficiencies of BPTU. Low carbon steel corrosion inhibition ability of BPTU is investigated at the temperature of 30, 40, 50, and 60°C. The results in Figure 8 show that, at the same concentration, as the temperature increases, the corrosion inhibition performances of BPTU decrease. Specifically, at 30°C, its inhibition efficiency reaches the highest value of 94.30% at 2×10^{-4} M (Table 2). However, these inhibition efficiencies are only 88.02% at 40°C, 66.15% at 50°C, and 54.01% at 60°C (Table 3). This can be explained that, as the temperature increases, BPTU molecules are desorbed from the steel surface, resulting in the reduction of inhibition performances.

3.4. Adsorption Isotherms. Adsorption isotherm models are used to study the behavior of inhibitors on the metal surface [39, 40]. In the present study, the Temkin, Freundlich, and Langmuir adsorption isotherms were chosen to appraise the nature of the interaction between BPTU molecules and low carbon steel surface in acidic solution.

The equation for the Temkin adsorption model is [41, 42]

$$\ln K_{ads} \cdot C = a \cdot \theta. \tag{11}$$

The Freundlich model is shown as follows [43]:

$$\log \theta = \log K_{ads} + n \log C. \tag{12}$$

The Langmuir model is represented in the following form [44]:

$$\frac{C}{\theta} = \frac{1}{K_{ads}} + C, \tag{13}$$

where K_{ads} is the equilibrium constant of the adsorption process, "a" is the lateral interaction term, and θ is surface coverage values. The value of n is used to describe the ease of adsorption.

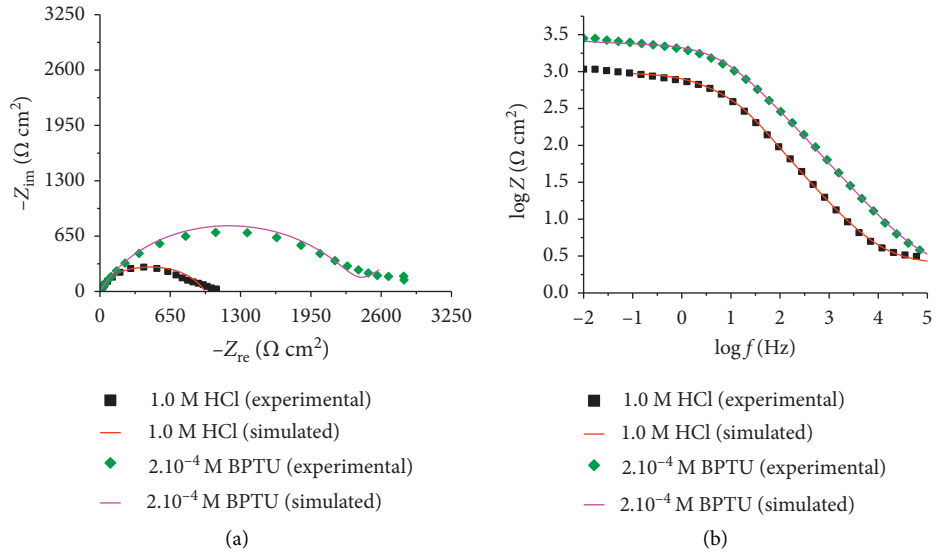

Figure 3: A representative of example simulation of (a) Nyquist and (b) Bode plots recorded for low carbon steel in 1.0 M HCl without and with 2.10^{-4} M BPTU.

Table 1: EIS parameters of low carbon steel in 1.0 M HCl with different concentrations of BPTU.

C_M (M)	R_{ct} (Ω cm^2)	R_s (Ω cm^2)	CPE ($\mu\Omega$ s^n cm^{-2})	n	C_{dl} (μF cm^{-2})	χ^2	H (%)
Blank	125 ± 1.21	3.52 ± 0.05	64.62 ± 1.54	0.80 ± 0.03	29.14 ± 2.12	0,0009	
2×10^{-4}	2495 ± 8.23	2.077 ± 0.07	13.19 ± 0.26	0.63 ± 0.02	4.20 ± 0.08	0,0008	94.99
10^{-4}	1652 ± 4.11	1.501 ± 0.04	14.03 ± 0.12	0.61 ± 0.02	5.07 ± 0.07	0,0002	92.43
5×10^{-5}	1374 ± 2.46	2.438 ± 0.06	22.4 ± 0.27	0.55 ± 0.01	5.24 ± 0.05	0,0008	90.90
10^{-5}	1018 ± 3.82	2.34 ± 0.05	24.51 ± 0.36	0.6 ± 0.03	6.11 ± 0.06	0,0009	87.72

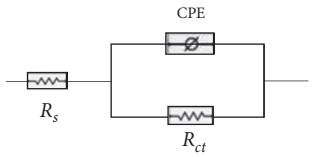

Figure 4: Equivalent circuit model of EIS.

Observing Figures 9 and 10, the correlation coefficients of the plot (R2) between ln$C$ vs θ and log C versus log θ are much different from the unit at 30°C. They prove that adsorptions of BPTU on low carbon steel surface do not conform Temkin and Freundlich isotherms. Langmuir adsorption is applied for the next evaluation (Figure 11). The plots exhibit the linearity with $R2$ values close to 1 for Langmuir. However, the slopes of these lines are different from the unit. To explain this phenomenon, Langmuir's adsorption isotherm is modified as follows [45, 46]:

$$\frac{C}{\theta} = \frac{M}{K_{ads}} + mC. \quad (14)$$

The factor "m" can be assumed to an inherent factor in the surface coverage values.

3.5. Adsorption Thermodynamic Parameters. The values of the adsorption constant (K_{ads}) are calculated from the slopes of the modified Langmuir adsorption isotherms (Table 4).

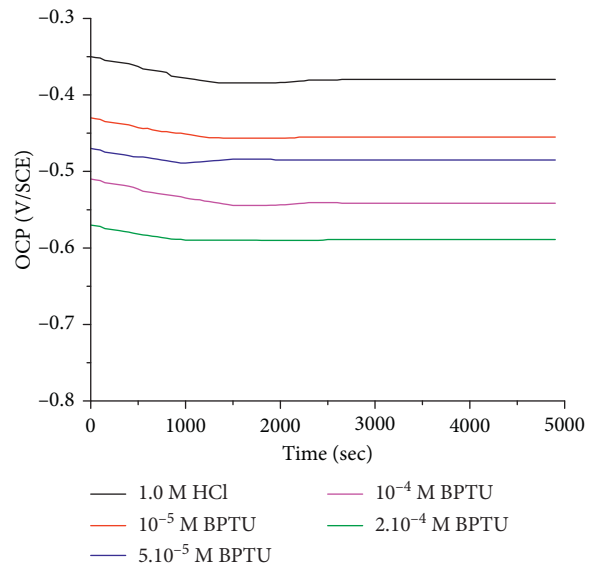

Figure 5: Open circuit potential for mild steel with different concentrations of BPTU.

Based on the relationship between K_{ads} and the free energy of adsorption ($\Delta\mathbf{G}^{\mathbf{0}}_{\mathbf{ads}}$) expressed in equation (7), $\Delta\mathbf{G}^{\mathbf{0}}_{\mathbf{ads}}$ is calculated in Table 4.

The van't Hoff equation is used to calculate the standard enthalpy of the adsorption process $\Delta\mathbf{H}^{\mathbf{0}}_{\mathbf{ads}}$:

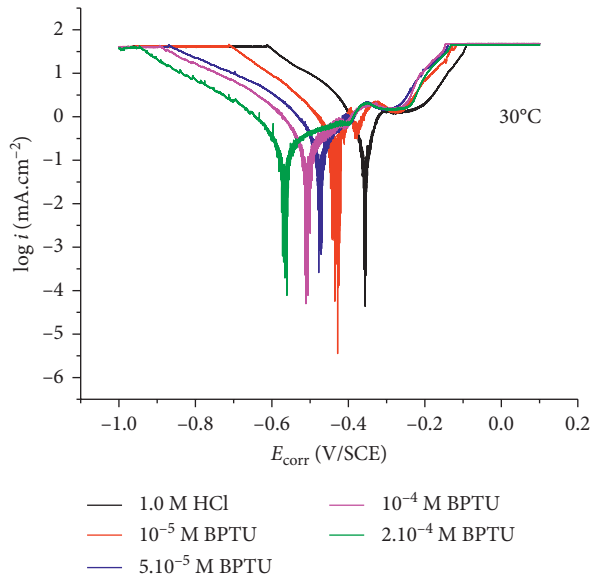

Figure 6: Potentiodynamic polarization curves of mild steel in 1.0 M HCl with different concentrations of BPTU at 30°C.

Table 2: Polarization curve parameters of low carbon steel in 1.0 M HCl with different concentrations of BPTU and URO at 30°C.

Inhibitors	Concentration (M)	i_{corr} (i_{inh}) (mA.cm^{-2})	β_a (mV.dec^{-1})	$-\beta_b$ (mV.dec^{-1})	H (%)
BPTU	Blank	0.9000	36.4	24.8	—
	2×10^{-4}	0.0513	32.8	32.5	94.30 (1.30)
	10^{-4}	0.0688	32.5	35.7	92.35 (1.25)
	5×10^{-5}	0.0885	32.9	39.4	90.16 (1.30)
	10^{-5}	0.1067	31.3	40.1	88.15 (1.40)
URO	2×10^{-4}	0.4809	33.9	35.5	46.57 (1.15)

*Values in parenthesis in the last column of this table are the mean absolute deviation.

$$\frac{d \ln K_{ads}}{dT} = \frac{\Delta H^0_{ads}}{RT}. \quad (15)$$

The equation can be changed [47]:

$$\ln K_{ads} = \frac{-\Delta H^0_{ads}}{RT} + A, \quad (16)$$

where A is integral constant.

The relationship between $\ln K_{ads}$ and 1/T is established and shown in Figure 12. The value of $\Delta \mathbf{H^0_{ads}}$ is calculated from the slope of these straight lines given in Table 4. The standard adsorption entropy ($\Delta \mathbf{S^0_{ads}}$) is figured out via equation (4).

The results in Table 4 reveal that $\Delta \mathbf{H^0_{ads}}$ values are negative which implies that the adsorption of BPTU on steel surface is an exothermic process. It is agreed that the value of $\Delta \mathbf{H^0_{ads}}$ is less negative than −40 kJ mol^{-1} (physisorption) and more negative than −100 kJ mol^{-1} (for chemisorption) [38]. $\Delta \mathbf{H^0_{ads}}$ of BPTU has a value of −39.68 kJ mol^{-1}; this indicates that BPTU molecules take part in the physisorption process on the steel surface. It is an electrostatic interaction between the charged inhibitors and charged steel. Therefore, they are easily separated from the metal surface when the temperature rises.

It is observed that $\Delta \mathbf{S^0_{ads}}$ values are positive with the presence of inhibitors. It is explained that entropy of the gas molecules adsorption on the steel surface has a negative value, but the adsorption of the inhibitor molecules in the solution is accompanied with the adsorption of cations and anions attached to the steel surface. The result leads to an increase in untidiness of the molecules on the steel surface. This is also an important driving force for inhibitor molecules adsorption [48].

3.6. Scanning Electron Microscopy (SEM) Analysis. Figure 13(a) is a SEM image of a low carbon steel surface without corrosion. In the absence of the inhibitor, the steel surface is strongly destroyed in 1.0 M HCl solution (Figure 13(b)). However, this surface is significantly protected with the presence of BPTU (Figure 13(c)). The pitting or crevice corrosion has been reduced. These prove that BPTU can inhibit the metal corrosion process in acidic solution by forming a molecular film on the low carbon steel surface, preventing the steel from the corrosive agents. This is in concordance with the high inhibition efficiency of BPTU obtaining from the mentioned electrochemical methods.

3.7. Quantum Chemical Calculations. Quantum chemical method based DFT calculations are carried out to determine the relationship between the structure and behavior of

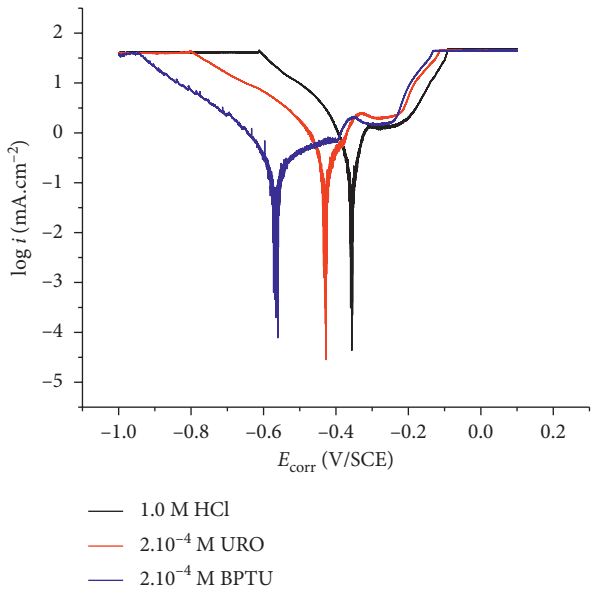

Figure 7: Potentiodynamic polarization curves of mild steel in 1.0 M HCl in the presence of BPTU and URO at 30°C.

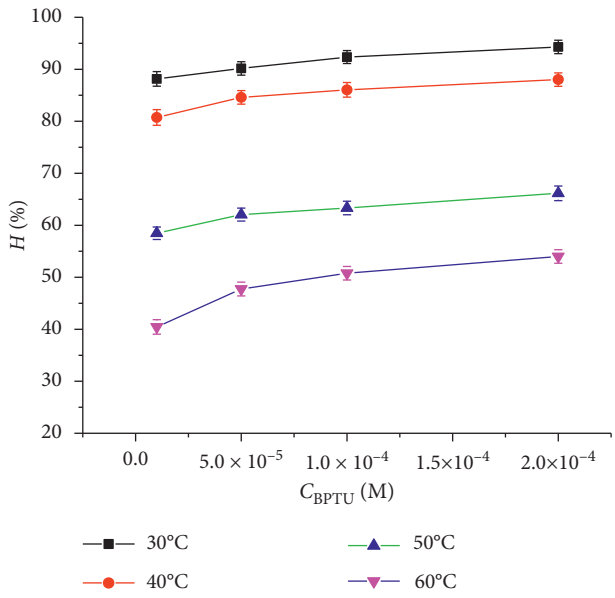

Figure 8: Relationship between concentrations and inhibition efficiencies of BPTU at the different temperatures.

corrosion inhibitors [49]. The optimized structures of BPTU and URO are conducted with B3LYP/6-311G(d,p) mode and atom numbered as Figure 14.

The adsorption centers of inhibitors are predicted through the Mülliken population analysis [50]. Sulfur and nitrogen atoms are more negative charges (Table 5); thus they are the easiest electron donation positions of BPTU, forming the donor-acceptor bond between BPTU and the iron surface. Besides, two benzene rings in BPTU contribute to the formation of the adsorbate-surface complex [51].

The highest occupied molecular orbital (HOMO) and lowest unoccupied molecular orbital (LUMO) can reveal the electron donating and accepting position of the molecule under favorable conditions [27, 28]. The HOMO electron density (in Figure 15) shows that BPTU can donate electron mainly in the positions of S, N atoms. In contrast, LUMO electron density indicates that receiving positions of BPTU are at the entire molecule.

Electronic parameters of BPTU including the energy of the highest occupied molecular orbital (E_{HOMO}), lowest unoccupied molecular orbital energy (E_{LUMO}), energy gap ($\Delta E_{L\text{-}H} = E_{LUMO} - E_{HOMO}$), chemical hardness ($\eta$), and chemical softness (S) are calculated and compared with quantum chemical parameters of URO (Table 6).

The high value of E_{HOMO} often relates to the strong electron giving ability of a molecule [27]. E_{HOMO} of BPTU (−5.61 eV) is higher than E_{HOMO} of URU (−6.04 eV); thus, the order of inhibition efficiency of BPTU and URO is arranged to be the same trend as E_{HOMO}.

E_{LUMO} is consistent with the electron accepting ability of the inhibitor molecules. The low value of E_{LUMO} is associated with strong metal-inhibitor bonding and thereby high protection ability. Based on the E_{LUMO} value, the inhibition efficiency of BPTU is higher than that of URO.

The energy gap is an important parameter that depicts the connection of molecules and the metal surface. The value of $\Delta E_{L\text{-}H}$ is small, and the molecule is much polar metal [52]. Thus, it can adsorb easily on the metal surface. In this work, BPTU has an energy gap value of 4.68 eV; it is smaller than this value of URO. Thus, BPTU is predictable to be a more excellent inhibitor than URO.

Chemical softness and chemical hardness are used to describe the stability and reactivity of the molecule. Hardness (η) characterizes the change of the chemical potential on the total number of atoms [30]. The low hardness value proves that it can take part in the reaction easily. In contrast, the chemical softness (S) represents the quantitative characteristic of electron cloud polarization in compounds [53]. Transfer of electron in easy way needs great softness value. The values of η and S show that BPTU is better than URO in terms of inhibiting the metal corrosion process.

In acid solution, inhibitors can undergo a protonation at the positions of heteroatoms (i.e., *N*, *S*). Therefore, their cationic forms should be investigated to determine the most stable configuration of inhibitor molecules in aggressive acidic solution. BPTU can be protonated at S1, N2, and N3 while this site is N for URO (pURO-N) (Figure 16). All protonated structures of both BPTU and URO are optimized at the theory level of B3LYP/6-311G(d,p). Their relative energy values comparing to pBPTU-S1 are demonstrated in parentheses. pBPTU-S1 has the lowest energy in protonated BPTU forms, so it is selected to compare with pURO-N.

In the case of protonation, the quantum chemical parameters of pBPTU-S1 and pURO-N are also calculated in Table 6. The obtained results show that pBPTU-S1 is better at inhibiting steel corrosion than pURO-N. This entirely supported the experimental results.

3.8. Molecular Dynamics Simulation. Adsorption of the inhibitor molecule on steel surface is simulated by modeling the interaction between the inhibitor molecules

Table 3: Polarization curve parameters of low carbon steel in 1.0 M HCl with different concentrations of BPTU at 40, 50, and 60°C***.

Temperatures (°C)	Concentration (M)	i_{corr} (i_{inh}) (mA.cm^{-2})	H%
40	Blank	1.0070	
	2×10^{-4}	0.1207	88.02 (1.30)
	10^{-4}	0.1405	86.05 (1.40)
	5×10^{-5}	0.1551	84.59 (1.32)
	10^{-5}	0.1940	80.73 (1.50)
50	Blank	4.1032	
	2×10^{-4}	1.3889	66.15 (1.40)
	10^{-4}	1.5051	63.32 (1.29)
	5×10^{-5}	1.5570	62.05 (1.25)
	10^{-5}	1.7039	58.48 (1.20)
60	Blank	7.3500	
	2×10^{-4}	3.3803	54.01 (1.28)
	10^{-4}	3.6177	50.78 (1.13)
	5×10^{-5}	3.8414	47.74 (1.32)
	10^{-5}	4.3766	40.45 (1.41)

**Values in parenthesis in the last column of this table are the mean absolute deviation.

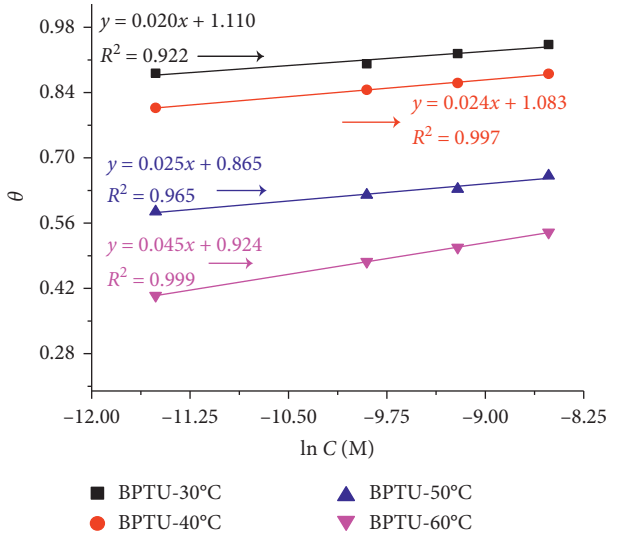

Figure 9: Temkin's adsorption isotherm of BPTU on the steel surface in 1.0 M HCl.

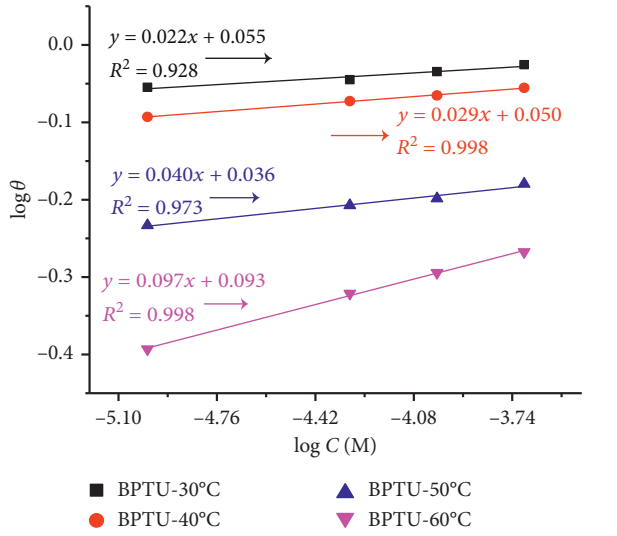

Figure 10: Freundlich's adsorption isotherm of BPTU on the steel surface in 1.0 M HCl.

and Fe (110) crystal surface in 1.0 M HCl solution. Figure 17 shows the side and top views of BPTU and URO adsorption in protonated and neutral forms. In general, the inhibitor molecules are close to the surface of Fe (110), so that they can cover the iron surface, preventing the contact of iron and corrosive agents in the solution. However, when comparing the adsorption configurations of neutral and protonated molecules, there is a difference between BPTU and URO. In the neutral form of BPTU, S atom is directed towards the surface of Fe (110) and it may donate its unpaired electron pairs to iron to form a coordination bond (Figure 17(a)). On the contrary, the SH group turns upwards against the iron surface in the adsorption configuration of protonated BPTU form (Figure 17(b)). In this case, benzene rings increase the electrostatic interaction between the inhibitor molecule and Fe (110) and N atoms give their undivided electron pairs into the vacant Fe orbitals to create coordination bonds. For URO, the adsorption configurations in neutral and protonated forms do not seem to change (Figures 17(c) and 17(d)).

Analysis of obtained results from molecular dynamics simulation in Table 7 shows that the binding energies of protonated inhibitors are higher than those of neutral molecules. This demonstrates that protonated inhibitors strongly bind to the Fe (110) surface. Besides, the more negative interaction energy of BPTU indicates the stronger interaction between BPTU and the iron surface when comparing to that of URO [54]. This is entirely consistent with the obtained experimental values.

3.9. Mechanism of Corrosion Inhibition. In the molecule of BPTU, there are two nitrogen atoms and one sulfur atom. They are positions which have high electron density due to flexible electron pairs, so BPTU is susceptibly protonated

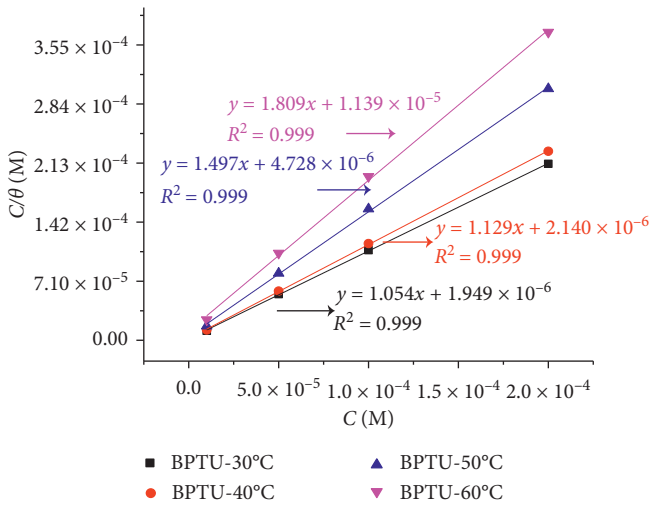

Figure 11: Langmuir's adsorption isotherm of BPTU on the steel surface in 1.0 M HCl.

Table 4: Adsorption parameters of BPTU in HCl solution.

Temperature (°C)	K_{ads} (M^{-1})	ΔG^0_{ads} (kJ mol^{-1})	ΔH^0_{ads} (kJ mol^{-1})	ΔS^0_{ads} (J $mol^{-1}K^{-1}$)
30	$10^{5.82}$	−43.86	−39.68	13.77
40	$10^{5.72}$	−44.74	−39.68	16.16
50	$10^{5.50}$	−44.80	−39.68	15.84
60	$10^{5.20}$	−44.27	−39.68	13.79

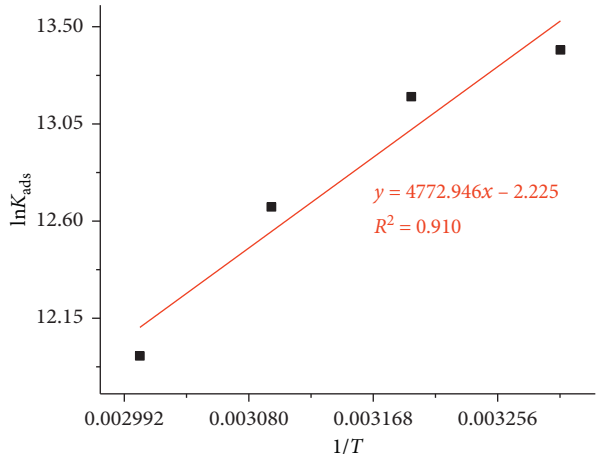

Figure 12: Relationship between ln K_{ads} and $1/T$ in 1.0 M HCl solution.

in acidic solution [55]. Meanwhile, Cl^- ions tend to move and adsorb onto the iron surface, making it charged negatively. Therefore, protonated BPTU physically adsorbs on the steel surface through electrostatic interaction [56]. Afterwards, H^+ ions receive electrons, H_2 gas is released, and BPTU is converted to the neutral state. The main adsorption center of BPTU which locates mainly in the thiourea group can donate electrons into empty d orbitals of iron atoms to form a coordinate-covalent bond through nucleophilic interaction. Two benzene rings in the BPTU molecule have a large coverage; they prevent the iron surface from corrosive agents in the acid solution. These characteristics make BPTU become a perfect corrosion inhibitor in acid.

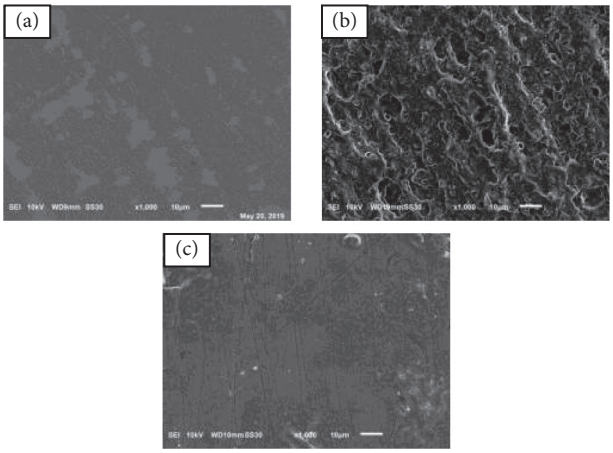

Figure 13: SEM images of low carbon steel surfaces (a) before corrosion, (b) in 1.0 M HCl, and (c) in 2.10^{-4} M BPTU.

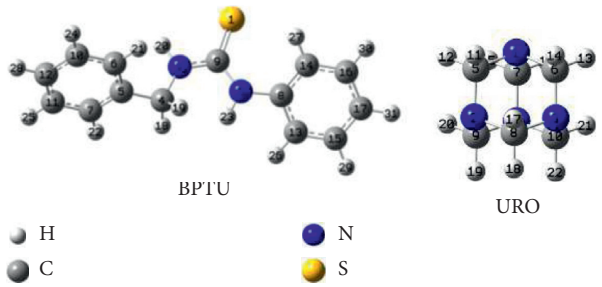

Figure 14: Optimized structures of BPTU and URO.

Table 5: Mülliken population of BPTU in gas phase.

Elements	S1	N2	N3	C4	C5	C6	C7	C8	C9
Charges	−0.276	−0.395	−0.456	−0.040	−0.165	−0.050	−0.059	0.182	0.187
Elements	C10	C11	C12	C13	C14	C15	C16	C17	
Charges	−0.087	−0.090	−0.084	−0.112	−0.045	−0.099	−0.108	−0.088	

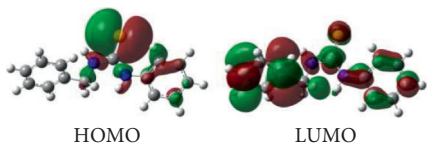

Figure 15: HOMO and LUMO of BPTU.

Table 6: Electronic parameters derived for neutral as well as protonated inhibitors.

Inhibitors	E_{HOMO} (eV)	E_{LUMO} (eV)	$\Delta E_{(L\text{-}H)}$ (eV)	η (eV)	S (eV^{-1})
BPTU	−5.61	−0.93	4.68	−3.27	2.34
URO	−6.04	0.88	6.92	3.46	0.29
pBPTU–S1	−10.04	−4.84	5.21	2.60	0.38
pURO–N	−11.05	−4.26	6.78	3.39	0.29

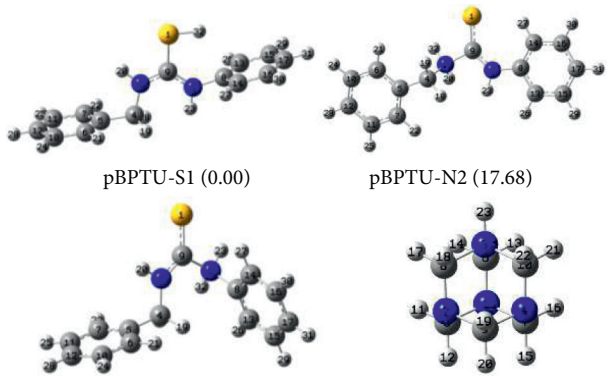

Figure 16: Optimized structures of protonated BPTU (pBPTU) and URO (pURO) (relative energies of protonated inhibitors comparing to the energy of pBPTU-S1 are shown in parentheses in kcal.mol^{-1}).

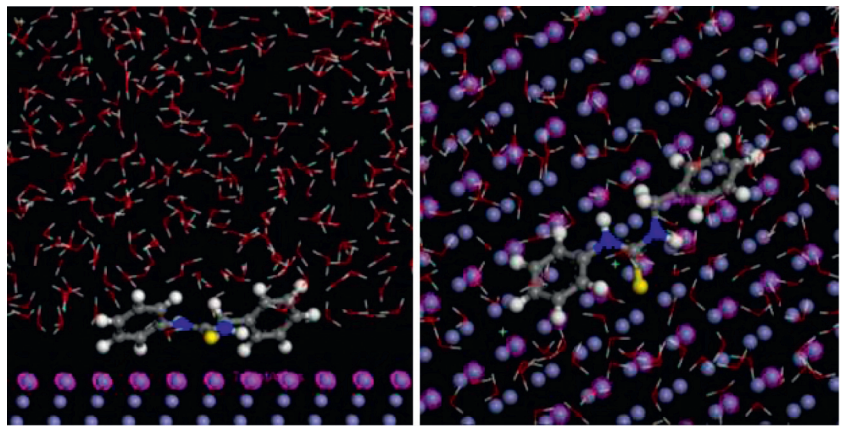

(a)

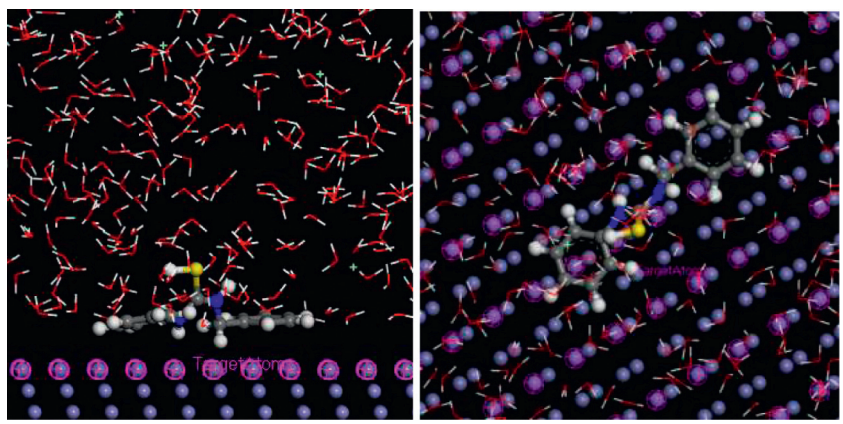

(b)

Figure 17: Continued.

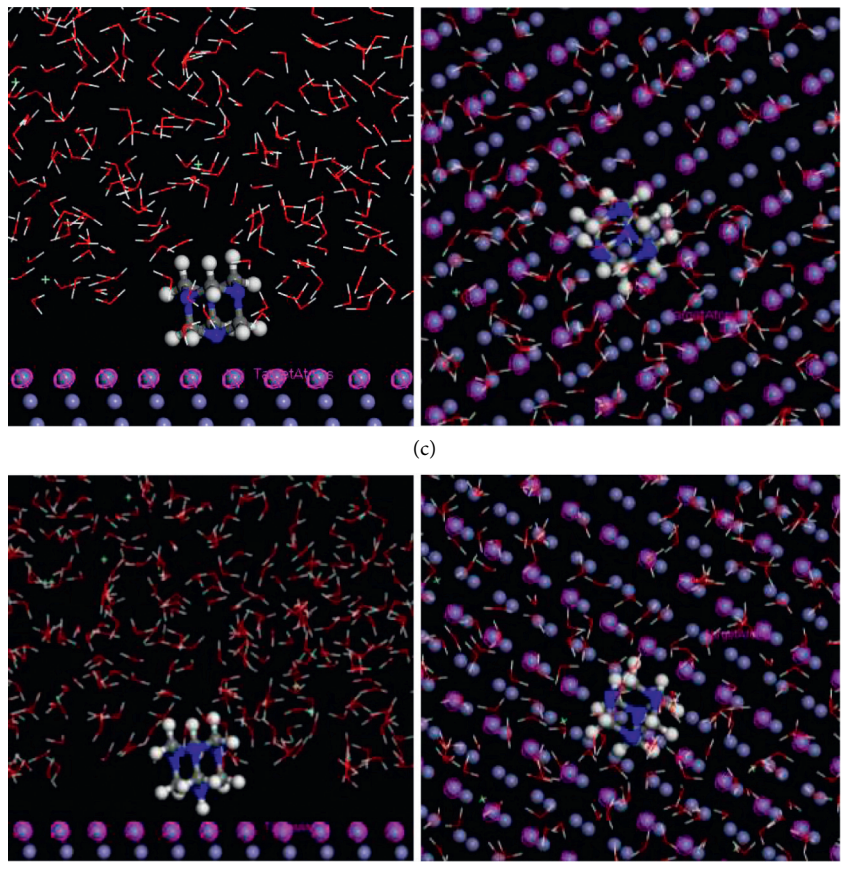

(c)

(d)

Figure 17: Configurations of (a) BPTU, (b) pBPTU-S1, (c) URO, and (d) pURO-N on Fe (110) surface in acidic solution.

Table 7: Energy values (kcal.mol^{-1}) of inhibitor molecule adsorption on the Fe (110) surface in acidic solution.

	E_{tot}	$E_{surf+sol}$	E_{inh}	E_{int}	E_{bind}
Fe (110) + BPTU	2114.98	2038.88	635.58	−559.48	559.48
Fe (110) + URO	2104.42	2038.88	617.55	−552.01	552.01
Fe (110) + pBPTU-S1	2116.06	2038.88	640.60	−563.42	563.42
Fe (110) + pURO-N	2105.64	2038.88	620.08	−553.32	553.32

4. Conclusions

Researching low carbon steel corrosion inhibition ability of BPTU in 1.0 M HCl solution by experimental methods and quantum chemical calculations, the results can be given as follows:

(1) BPTU can protect the steel in acid solution with the highest efficiency of 94.99% from EIS and 94.30% from PPM at 2×10^{-4} M and 30°C.

(2) BPTU can inhibit the steel corrosion better than URO—a traditional inhibitor.

(3) The higher the temperature, the lower the steel corrosion inhibition ability of BPTU.

(4) The adsorption of BPTU on steel surface does not follow the Temkin and Freudlich isotherm adsorption models, obeying the modified Langmuir isotherm adsorption model.

(5) SEM analysis results reveal that BPTU protects the steel surface quite effectively by forming a protective film.

(6) Theoretical calculations demonstrate that the reactive sites of BPTU are S, N with unpaired electrons and these results are completely in accordance with the experimental findings.

Data Availability

The data used to support this study are included in the supplementary information.

Conflicts of Interest

The authors declare that there are no conflicts of interest.

Acknowledgments

This work was financially supported by the Science and Technology Research Fund of Hue University under Grant no. DHH2020-03-135.

Supplementary Materials

Here are some additional data about the electric structures of BPTU and URO in stable neutral and protonated forms (Tables S1, S2, S3). These data are provided to help readers better understand the configurations of compounds optimized at the B3LYP/6-311G(d,p) level of theory. Table S1: optimized structure of BPTU in the gas phase using B3LYP/6-311G(d,p). Table S2: optimized structure of URO in the gas phase using B3LYP/6-311G(d,p). Table S3: optimized structures of protonated BPTU (pBPTU) and URO (pURO) in the gas phase using B3LYP/6-311G(d,p). (*Supplementary Materials*)

References

[1] R. Agrawal and T. K. G. Namboodhiri, "The inhibition of sulphuric acid corrosion of 410 stainless steel by thioureas," *Corrosion Science*, vol. 30, no. 1, pp. 37–52, 1990.

[2] X. L. Cheng, H. Y. Ma, S. H. Chen, R. Yu, X. Chen, and Z. M. Yao, "Corrosion of stainless steels in acid solutions with organic sulfur-containing compounds," *Corrosion Science*, vol. 41, no. 2, pp. 321–333, 1998.

[3] A. Frignani, C. Monticelli, and F. Zucchi, "Inhibiting action of phenylthiourea towards iron-based metallic glass corrosion in acid environment," *Materials Chemistry and Physics*, vol. 92, no. 2-3, pp. 403–407, 2005.

[4] M. Özcan, İ. Dehri, and M. Erbil, "Organic sulphur-containing compounds as corrosion inhibitors for mild steel in acidic media: correlation between inhibition efficiency and chemical structure," *Applied Surface Science*, vol. 236, no. 1-4, pp. 155–164, 2004.

[5] S. Malinowski, J. Jaroszynska-Wolinska, and T. Herbert, "Theoretical predictions of anti-corrosive properties of THAM and its derivatives," *Journal of Molecular Modeling*, vol. 24, no. 1, pp. 1–12, 2017.

[6] X. Li, S. Deng, and H. Fu, "Allyl thiourea as a corrosion inhibitor for cold rolled steel in H 3 PO 4 solution," *Corrosion Science*, vol. 55, pp. 280–288, 2012.

[7] V. V. Torres, V. A. Rayol, M. Magalhães et al., "Study of thioureas derivatives synthesized from a green route as corrosion inhibitors for mild steel in HCl solution," *Corrosion Science*, vol. 79, pp. 108–118, 2014.

[8] L. Guo, S. Kaya, I. B. Obot, X. Zheng, and Y. Qiang, "Toward understanding the anticorrosive mechanism of some thiourea derivatives for carbon steel corrosion: a combined DFT and molecular dynamics investigation," *Journal of Colloid and Interface Science*, vol. 506, pp. 478–485, 2017.

[9] A. S. Fouda and A. H. Soliman, "Corrosion protection of carbon steel in hydrochloric acid solutions using thiourea derivatives," *Protection of Metals and Physical Chemistry of Surfaces*, vol. 51, no. 5, pp. 847–860, 2015.

[10] Y. Yan, L. Dai, L. Zhang et al., "Investigation on the corrosion inhibition of two newly-synthesized thioureas to mild steel in 1 mol/L HCl solution," *Research on Chemical Intermediates*, vol. 44, no. 5, pp. 3437–3454, 2018.

[11] D. Q. Huong, T. Duong, and P. C. Nam, "Experimental and theoretical study of corrosion inhibition performance of N-phenylthiourea for mild steel in hydrochloric acid and sodium chloride solution," *Journal of Molecular Modeling*, vol. 25, no. 7, p. 204, 2019.

[12] A. G. Brolo, M. L. A. Temperini, and S. M. L. Agostinho, "Effect of hexamethylenetetramine as a corrosion inhibitor for copper in bromide medium," *Journal of Electroanalytical Chemistry*, vol. 335, no. 1-2, pp. 83–92, 1992.

[13] E. Bayol, K. Kayakırılmaz, and M. Erbil, "The inhibitive effect of hexamethylenetetramine on the acid corrosion of steel," *Materials Chemistry and Physics*, vol. 104, no. 1, pp. 74–82, 2007.

[14] M. Hosseini, S. F. L. Mertens, and M. R. Arshadi, "Synergism and antagonism in mild steel corrosion inhibition by sodium dodecylbenzenesulphonate and hexamethylenetetramine," *Corrosion Science*, vol. 45, no. 7, pp. 1473–1489, 2003.

[15] D. D. N. Singh, T. B. Singh, and B. Gaur, "The role of metal cations in improving the inhibitive performance of hexamine on the corrosion of steel in hydrochloric acid solution," *Corrosion Science*, vol. 37, no. 6, pp. 1005–1019, 1995.

[16] B. Ngouné, M. Pengou, A. M. Nouteza, C. P. Nanseu-Njiki, and E. Ngameni, "Performances of alkaloid extract from rauvolfia macrophylla stapf toward corrosion inhibition of C38 steel in acidic media," *ACS Omega*, vol. 4, no. 5, pp. 9081–9091, 2019.

[17] N. Uzma, A. Zareen, and J. N. Kausar, "Biferrocenyl Schiff bases as efficient corrosion inhibitors for an aluminium alloy in HCl solution: a combined experimental and theoretical study," *RSC Advances*, vol. 10, no. 13, pp. 7585–7599, 2020.

[18] Y. Koumya, R. Idouhli, A. Oukhrib, M. Khadiri, A. Abouelfida, and A. Benyaich, "Synthesis, electrochemical, thermodynamic, and quantum chemical investigations of amino cadalene as a corrosion inhibitor for stainless steel type 321 in sulfuric acid 1 M," *International Journal of Electrochemistry*, vol. 2020, pp. 1–10, 2020.

[19] J. Haque, V. Srivastava, D. S. Chauhan, H. Lgaz, and M. A. Quraishi, "Microwave-induced synthesis of chitosan schiff bases and their application as novel and green corrosion inhibitors: experimental and theoretical approach," *ACS Omega*, vol. 3, no. 5, pp. 5654–5668, 2018.

[20] C. H. Hsu and F. Mansfeld, "Technical note: concerning the conversion of the constant phase element parameter Y0 into a capacitance," *Corrosion*, vol. 57, no. 9, pp. 747-748, 2001.

[21] Y. Yan, W. Li, L. Cai, and B. Hou, "Electrochemical and quantum chemical study of purines as corrosion inhibitors for mild steel in 1 M HCl solution," *Electrochimica Acta*, vol. 53, no. 20, pp. 5953–5960, 2008.

[22] K. Peipei, F. Huixia, and C. Nali, "Polyaniline/chitosan as a corrosion inhibitor for mild steel in acidic medium," *RSC Advances*, vol. 9, no. 16, pp. 9211–9217, 2019.

[23] M. Behpour, S. M. Ghoreishi, N. Mohammadi, N. Soltani, and M. Salavati-Niasari, "Investigation of some Schiff base compounds containing disulfide bond as HCl corrosion inhibitors for mild steel," *Corrosion Science*, vol. 52, no. 12, pp. 4046–4057, 2010.

[24] A. K. Singh, S. Thakur, B. Pani, E. E. Ebenso, M. A. Quraishi, and A. K. Pandey, "2-Hydroxy-N′-((Thiophene-2-yl)methylene)benzohydrazide: ultrasound-assisted synthesis and corrosion inhibition study," *ACS Omega*, vol. 3, no. 4, pp. 4695–4705, 2018.

[25] R. Aslam, M. Mobin, S. Zehra, I. B. Obot, and E. E. Ebenso, "N,N′-Dialkylcystine gemini and MonomericN-alkyl cysteine surfactants as corrosion inhibitors on mild steel corrosion in 1 M HCl solution: a comparative study," *ACS Omega*, vol. 2, no. 9, pp. 5691–5707, 2017.

[26] M. J. Frisch, G. W. Trucks, and H. B. Schlegel, *Gaussian 09*, Gaussian, Inc., Wallingford CT, USA, 2009.

[27] N. Khalil, "Quantum chemical approach of corrosion inhibition," *Electrochimica Acta*, vol. 48, no. 18, pp. 2635–2640, 2003.

[28] S. Deng, X. Li, and X. Xie, "Hydroxymethyl urea and 1,3-bis(hydroxymethyl) urea as corrosion inhibitors for steel in HCl solution," *Corrosion Science*, vol. 80, pp. 276–289, 2014.

[29] H. Chermette, "Chemical reactivity indexes in density functional theory," *Journal of Computational Chemistry*, vol. 20, no. 1, pp. 129–154, 1999.

[30] E. E. Ebenso, D. A. Isabirye, and N. O. Eddy, "Adsorption and quantum chemical studies on the inhibition potentials of some thiosemicarbazides for the corrosion of mild steel in acidic medium," *International Journal of Molecular Sciences*, vol. 11, no. 6, pp. 2473–2498, 2010.

[31] F. Conforti, S. Sosa, M. Marrelli et al., "In vivo anti-inflammatory and in vitro antioxidant activities of Mediterranean dietary plants," *Journal of Ethnopharmacology*, vol. 116, no. 1, pp. 144–151, 2008.

[32] D. S. Biovia, *Materials Studio, Revision 8.0*, Accelrys, San Diego, CA, USA, 2017.

[33] Z. Salarvand, M. Amirnasr, M. Talebian, K. Raeissi, and S. Meghdadi, "Enhanced corrosion resistance of mild steel in 1 M HCl solution by trace amount of 2-phenyl-benzothiazole derivatives: experimental, quantum chemical calculations and molecular dynamics (MD) simulation studies," *Corrosion Science*, vol. 114, pp. 133–145, 2017.

[34] S. K. Saha, P. Ghosh, A. Hens, N. C. Murmu, and P. Banerjee, "Density functional theory and molecular dynamics simulation study on corrosion inhibition performance of mild steel by mercapto-quinoline Schiff base corrosion inhibitor," *Physica E: Low-Dimensional Systems and Nanostructures*, vol. 66, pp. 332–341, 2015.

[35] H. Lgaz, S. Masroor, M. Chafiq et al., "Evaluation of 2-mercaptobenzimidazole derivatives as corrosion inhibitors for mild steel in hydrochloric acid," *Metals*, vol. 10, no. 3, p. 357, 2020.

[36] O. Benali, L. Larabi, S. M. Mekelleche, and Y. Harek, "Influence of substitution of phenyl group by naphthyl in a diphenylthiourea molecule on corrosion inhibition of cold-rolled steel in 0.5 M H2SO4," *Journal of Materials Science*, vol. 41, no. 21, pp. 7064–7073, 2006.

[37] M. A. Deyab, A. S. Fouda, M. M. Osman, and S. Abdel-Fattah, "Mitigation of acid corrosion on carbon steel by novel pyrazolone derivatives," *RSC Advances*, vol. 7, no. 71, pp. 45232–45240, 2017.

[38] W. Zhang, H.-J. Li, Y. Wang, Y. Liu, Q.-Z. Gu, and Y.-C. Wu, "Gravimetric, electrochemical and surface studies on the anticorrosive properties of 1-(2-pyridyl)-2-thiourea and 2-(imidazol-2-yl)-pyridine for mild steel in hydrochloric acid," *New Journal of Chemistry*, vol. 42, no. 15, pp. 12649–12665, 2018.

[39] G. Moretti, G. Quartarone, A. Tassan, and A. Zlngales, "5-Amino- and 5-chloro-indole as mild steel corrosion inhibitors in 1 N sulphuric acid," *Electrochimica Acta*, vol. 41, no. 13, pp. 1971–1980, 1996.

[40] M. Lebrini, M. Lagrenée, H. Vezin, M. Traisnel, and F. Bentiss, "Experimental and theoretical study for corrosion inhibition of mild steel in normal hydrochloric acid solution by some new macrocyclic polyether compounds," *Corrosion Science*, vol. 49, no. 5, pp. 2254–2269, 2007.

[41] M. Hosseini, S. F. L. Mertens, M. Ghorbani, and M. R. Arshadi, "Asymmetrical schiff bases as inhibitors of mild steel corrosion in sulphuric acid media," *Materials Chemistry and Physics*, vol. 78, no. 3, pp. 800–808, 2003.

[42] A. E.-A. E.-S. Fouda and A. Hussein, "Role of some phenylthiourea derivatives as corrosion inhibitors for carbon steel in HCl solution," *Journal of the Korean Chemical Society*, vol. 56, no. 2, pp. 264–273, 2012.

[43] A. M. Al-Turkustani, S. T. Arab, and R. H. Al-Dahiri, "Aloe plant extract as environmentally friendly inhibitor on the corrosion of aluminum in hydrochloric acid in absence and presence of iodide ions," *Modern Applied Science*, vol. 4, no. 5, 2010.

[44] X. Zhou, H. Yang, and F. Wang, "[BMIM]BF4 ionic liquids as effective inhibitor for carbon steel in alkaline chloride solution," *Electrochimica Acta*, vol. 56, no. 11, pp. 4268–4275, 2011.

[45] E. O. Emeka, "Corrosion inhibitive effect and adsorption behaviour of hibiscus sabdariffa extract on mild steel in acidic media," *Portugaliae Electrochimica Acta*, vol. 26, pp. 303–314, 2008.

[46] L. Larabi, O. Benali, and Y. Harek, "Corrosion inhibition of copper in 1 M HNO3 solution by N-Phenyl oxalic dihydrazide and oxalic N-Phenylhydrazide N′-Phenylthiosemicarbazide," *Portugaliae Electrochimica Acta*, vol. 24, no. 3, pp. 337–346, 2006.

[47] L. Tang, G. Mu, and G. Liu, "The effect of neutral red on the corrosion inhibition of cold rolled steel in 1.0 M hydrochloric acid," *Corrosion Science*, vol. 45, no. 10, pp. 2251–2262, 2003.

[48] X. Li, S. Deng, H. Fu, and T. Li, "Adsorption and inhibition effect of 6-benzylaminopurine on cold rolled steel in 1.0 M HCl," *Electrochimica Acta*, vol. 54, no. 16, pp. 4089–4098, 2009.

[49] G. Gece, "The use of quantum chemical methods in corrosion inhibitor studies," *Corrosion Science*, vol. 50, no. 11, pp. 2981–2992, 2008.

[50] I. B. Obot, D. D. Macdonald, and Z. M. Gasem, "Density functional theory (DFT) as a powerful tool for designing new organic corrosion inhibitors. Part 1: an overview," *Corrosion Science*, vol. 99, pp. 1–30, 2015.

[51] R. L. Camacho-Mendoza, E. Gutiérrez-Moreno, E. Guzmán-Percástegui et al., "Density functional theory and electrochemical studies: structure-efficiency relationship on corrosion inhibition," *Journal of Chemical Information and Modeling*, vol. 55, no. 11, pp. 2391–2402, 2015.

[52] T. Ibrahim, E. Gomes, I. B. Obot, M. Khamis, and M. Abou Zour, "Corrosion inhibition of mild steel byCalotropisproceraleaves extract in a CO2saturated sodium chloride solution," *Journal of Adhesion Science and Technology*, vol. 30, no. 23, pp. 2523–2543, 2016.

[53] R. G. Parr and R. G. Pearson, "Absolute hardness: companion parameter to absolute electronegativity," *Journal of the American Chemical Society*, vol. 105, no. 26, pp. 7512–7516, 1983.

[54] B. Xu, Y. Ji, X. Zhang, X. Jin, W. Yang, and Y. Chen, "Experimental and theoretical studies on the corrosion inhibition performance of 4-amino-N,N-di-(2-pyridylmethyl)-aniline on mild steel in hydrochloric acid," *RSC Advances*, vol. 5, no. 69, pp. 56049–56059, 2015.

[55] C. A. Mann, B. E. Lauer, and C. T. Hultin, "Organic inhibitors of corrosion aromatic amines," *Industrial & Engineering Chemistry*, vol. 28, no. 9, pp. 1048–1051, 1936.

[56] N. Yilmaz, A. Fitoz, ÿ. Ergun, and K. C. Emregül, "A combined electrochemical and theoretical study into the effect of 2-((thiazole-2-ylimino)methyl)phenol as a corrosion inhibitor for mild steel in a highly acidic environment," *Corrosion Science*, vol. 111, pp. 110–120, 2016.